COMPENSATION OF PERTURBATIVE EFFECTS ON A THRUST MEASUREMENT MEMS PROBE FOR ELECTRIC PROPULSION

Conference Paper · August 2021

DOI: 10.1109/DTIP54218.2021.9568665

3 authors, including:

Séverin Astruc
Office National d'Études et de Recherches Aérospatiales
3 PUBLICATIONS **77** CITATIONS
SEE PROFILE

Paul-Quentin Elias
Office National d'Études et de Recherches Aérospatiales
56 PUBLICATIONS **846** CITATIONS
SEE PROFILE

COMPENSATION OF PERTURBATIVE EFFECTS ON A THRUST MEASUREMENT MEMS PROBE FOR ELECTRIC PROPULSION

ASTRUC Severin
DPHY, ONERA, Université Paris Saclay
F-91123 Palaiseau - FRANCE
severin.astruc@onera.fr

ELIAS Paul-Quentin
DPHY, ONERA, Université Paris Saclay
F-91123 Palaiseau - FRANCE
paul-quentin.elias@onera.fr

LEVY Raphael
DPHY, ONERA, Université Paris Saclay
F-92322 Châtillon - FRANCE
raphael.levy@onera.fr

***Abstract*— A quartz force sensor is being developed to measure the thrust of an electron cyclotron resonance (ECR) plasma thruster. This microelectromechanical system (MEMS) is immersed in the plasma jet produced by the thruster. At this location, it is subject to thermal heating, ion sputtering, and electrostatic charging effects. It also creates a Debye sheath that can change the thrust measurement. These perturbations cause a drift in the force measurement. Using a Finite-Element modeling of the MEMS probe, several sensor designs have been simulated in order to test different methods for reducing the thermal thrust drift. The use of an additional electrode on the sensor can reduce the effect of temperature gradient across the sensor by an order of magnitude. Moreover, a quartz temperature sensor enable to compensate the offset. Numerical simulations show that the thrust drift is reduced by 50% with this method.**

Keywords—Electric Propulsion, Thrust, Accelerometer, MEMS, Quartz, Plasma

I. INTRODUCTION

The use of Electric Propulsion (EP) is rising among the spacecraft propulsion systems. In EP, a plasma is formed to produce ions and electrons, which are ejected to produce a thrust. Owing to the large ejection velocity it enables, it provides a better use of propellant than chemical systems, thus reducing the weight of the satellite. However, the thrust being smaller than conventional chemical propulsion, it requires longer firings to obtain the same change of velocity. The qualification of these systems requires ground tests to demonstrate the performance over all the thruster lifetime (up to 10 000 hours of operation). Traditionally, one uses thrust balances [1] to measure this thrust (in the µN to mN range). A typical balance is fixed on the vacuum facility on one side, and it supports the thruster on the other side. For example, the ONERA set up can measure thrust as low as the tenth of µN [2]. Unfortunately, some ground test, including cold start tests and periodic thermal change, use large thermal panel incompatible with the pendulum. Moreover, the balances are often on the vacuum facility-dependent and they are not usable in space to compare ground and flight performances.

New sensors emerge to circumvent these issues. They are designed to be immersed in the plasma jet. In this case, sensors are physically decoupled from the thruster. Among these new sensors are the target pendulum. The plasma impinges on the target and induces a deflection, like a pendulum. A device measures the angle of the deflection. The target can be as large as the vacuum-facility to intercept most of the plasma jet [3]. A laser displacement sensor can easily measure the deflection to retrieve directly the thrust. However, the target can be significantly intrusive and modify the thruster properties. Smaller probes [4] are less intrusive. They measure pressure, which give the thrust through a scan on the plasma section. Unfortunately, these sensors are subject to thermal heating, ion sputtering and electrostatic charging effects [5].

We proposed to use an accelerometer developed at the ONERA as a small target [5] to perform thrust measurement for a 30W electron cyclotron resonance (ECR) ion thruster [6]. The first studies showed that the measure of the thrust is feasible but the accelerometer was subject to various significant measurement bias not adapted for this kind of measurement. In particular, the error of measurement were great because of the local thermal heating and electrostatic charging effects. In this work, we use a more precise and more sensitive quartz accelerometer developed by ONERA enabling thermal compensation, shown in Fig. 1. We study different designs from this accelerometer to measure the thrust and address the thermal issues.

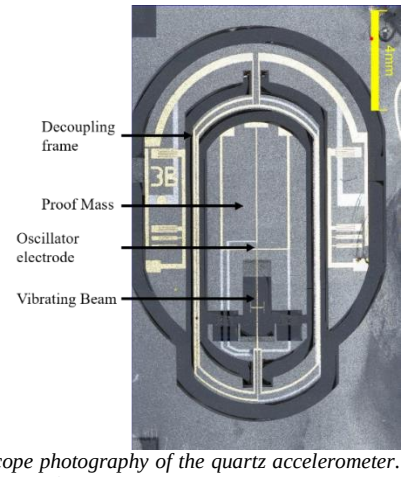

Fig. 1. Microscope photography of the quartz accelerometer. There is 3 gold electrodes used for the accelerometer quartz oscillator and 3 other gold electrodes used for a temperature quartz sensor.

II. ACCELEROMETER DESIGN

The quartz accelerometer is made from a 500µm thick monolithic α-quartz wafer. Its performances are described in the reference [7]. It is composed of a 2.5mm long vibrating beam linked to a proof mass and fixed to a decoupling frame, as shown in Fig. 1. Two hinges link directly the decoupling frame to the proof mass leaving only one degree of freedom for the proof mass as a pendulum, Fig. 2. An oscillator controls the beam vibration frequency (piezoelectric effect). The plasma will induce a force on the proof mass, rotating it round the hinge, which results in a constraint on the beam. The frequency of the beam increases depending on the force, as shown in (1).

$$\boldsymbol{\nu = \nu_0 + K_1 F + K_2 F^2 + \nu(T)} \qquad (1)$$

Where ν is the loaded vibrating beam frequency, ν_0 is the unloaded initial vibrating beam frequency, K_1 and K_2 are the linear and quadratic sensor scale factor in hertz by newton, and $\nu(T)$ is the dependency of the sensor in the temperature.

Quartz has low thermal expansion. Nonetheless, changes in size of the vibrating beam and the proof mass due to thermal heating add constraints in the vibrating beam and it increases the frequency measured with the term $\nu(T)$ in (1).

The use of an additional quartz temperature sensor mounted directly on the vibrating beam provides the beam temperature [8]. This sensor uses another oscillator of frequency $\nu_{\text{torsionnal}} = 640\text{kHz}$. It exploits the anisotropic quartz thermal expansion properties to compensate the temperature gradient in the thrust measurement. The flexure temperature sensibility S_{flexure} of the quartz is low compared to the torsional one $S_{\text{torsional}}$. The knowledge of the temperature sensibilities of the quartz enables to reduce the thermal drift on the measured force.

$$\boldsymbol{\nu_{corrected} = \nu - S_{flexure} \Delta T_{measured}}$$

Where $T_{\text{measured}} = \frac{\Delta\nu_{\text{torsional}}}{S_{\text{torsional}}}$ is the temperature measured by the quartz temperature sensor.

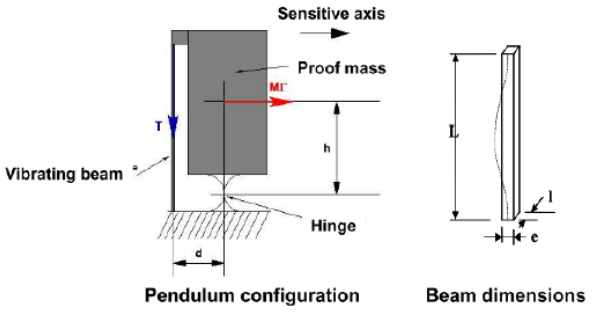

Fig. 2. Description of the working principle of the accelerometer. A force is acting upon the proof mass, which rotate round the hinge. The vibrating beam, maintained between the proof mass and the fixed part, is constrained and its fundamental frequency increase.

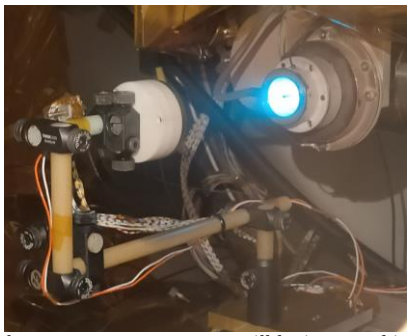

Fig. 3. The thrust measurement sensor will be immersed into the plasma jet on a cylindrical arm with other diagnostic probe. Here, only Langmuir probe is mounted on the arm in front of the ECR thruster powered on.

For the plasma pressure measurement, the sensor is immersed in front of the plasma thruster at a known position x, Fig. 3. The fundamental frequency ν_0, given in TABLE I. , is measured. Then, the thruster is powered on, and the sensor is subject to a frequency change $\Delta\nu = \nu_x - \nu_0$. As stated in (1), it depends on the change of force F_x applied on the proof mass and the effect of temperature. If the quadratic effect is neglected, this change in frequency can be written $\Delta\nu = K_1 F_x + \nu(T) = K_1 S P_x + \nu(T)$, where S is the surface of the proof mass and P_x is the local pressure created by the plasma jet. By scanning the plasma jet, one can integrate the pressure to retrieve the thrust of the thruster.

III. METHODOLOGY

Using a Finite-Element modeling of the MEMS probe, the effects of the thermal load on the thrust measurement are simulated thanks to the software OOFELIE::Multiphysics©. Different designs are tested to reduce the thermal drift of the sensor and the electrostatic effects, which both translates into a thrust drift. These designs include metal electrodes and a temperature sensor on the beam as described above. The goal of the simulation is to evaluate the resonant frequency of the different design with and without the thermal load.

A. Designs

Four designs have been studied as shown in Fig. 4: one reference model without metal electrode, one with the electrode on both side of the proof mass (I), one with the proof mass and the decoupling frame metallized (II) and one completely metallized (III). The designs I to III include a metal electrode. It is a 200 nanometers layer of gold deposited on the quartz. This electrode is necessary to collect and evacuate the ion charges, thus, decreasing the electrostatic force between the proof mass and its metallic case. It may also improve conductive cooling.

TABLE I. PROPERTIES OF THE QUARTZ ACCELEROMETER

	Unit	**Performances**
Frequency ν_0	kHz	33
Torsional frequency	kHz	640
Scale factor $K_1 S$	Hz/(µN.cm^{-2})	0.291
Proof Mass Surface S	mm²	15

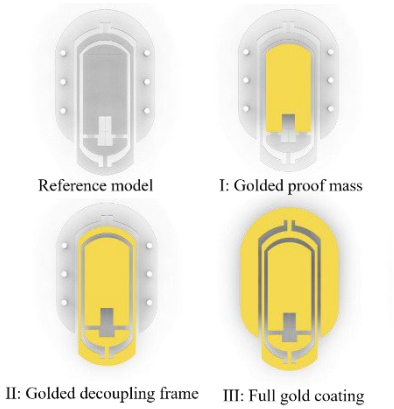

Fig. 4. The different designs used evaluated under thermal load. The reference model is a quartz sensor, the model I to III have different layer of gold. These layers are the same on the top and on the bottom of the models.

B. *Simulation Input*

The MEMS is subject to thermal load from the ion thruster. In operation, most of the sensor is protected and the ionic jet will only affect the proof mass. Because of the vacuum, only conductive and radiative heat transfers cool the MEMS, as depicted in

Fig. 5. The conductive transfer occurs only through the pads which link mechanically the quartz crystal to the casing while radiative cooling is applied on all surfaces.

C. *Simulation*

Each design is studied through a modal analysis to determine the resonance frequencies of the vibrating beam. It is chained with a static thermomecanical analysis where a thermal load is then applied to determine the temperature constraint on the sensor. Then a prestressed modal analysis is used to compute the change in frequency.

IV. INPUT VALUE

The effect of the temperature depends on the thermal load and the radiative and conductive cooling. The thermal load is simulated in the Finite-Element code with a heat flux applied on exposed part of the proof mass.

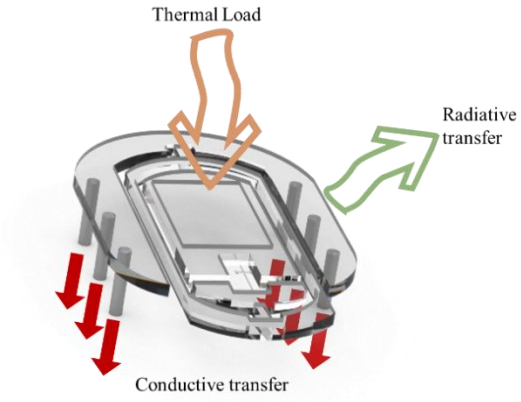

Fig. 5. Thermal transfers occurring when the plasma hits the sensor. A thermal load heat the proof mass over a surface Σ_p. Radiative cools the sensor via its entire surface Σ_{RT} and conductive transfer cools the quartz through the long pad.

By hypothesis, ions from the thruster give all of their kinetic energy to the proof mass at the impact. Secondary emission, which will reduce the heat flux is not taken into account. Thus, the thermal flux q_p'' can be computed with (2).

$$\boldsymbol{q_p'' = J.E_{Xe}\ (W.cm^2)} \qquad (2)$$

Where J ($A.cm^2$) is the ionic current and E_{Xe}(eV) is the mean ion kinetic energy.

The ion current has been measured at 20cm in front of the thruster, $J = 0.248\ mA.cm^{-2}$. From [9], ion energy after 10cm is $E_{Xe} = 170$ eV wich gives a velocity of 16km/s. Thus, the thermal load of the thruster on the proof mass at 20cm is $q_p'' = 43 mW.cm^{-2}$.

Radiative cooling flux q_{RT}'' occur on all the faces of the sensor. The Stefan-Boltzmann law (3) depend of the emissivity ε of the material.

$$\boldsymbol{q_{RT}'' = \sigma\varepsilon\left(T^4 - T_0^4\right)} \qquad (3)$$

Where σ is the Stefan-Boltzmann constant, T is the temperature of the sample and T_0 is the temperature of the casing.

The emissivity depends greatly of the surface material. An experiment has been conducted to determine this coefficient. Two 500µm thick quartz samples, one uncoated and one with a layer of gold on its surface are placed in front of the ion thruster. On the backside of the samples, a PT100 temperature sensor is glued. These samples are fixed to a copper support with kapton tape and a bolt. The contact surface between the quartz sample and the copper support represents 10% of the surface of the sample.

Applying the law of conservation of the energy on the sample, one gets:

$$\boldsymbol{\rho C_p \frac{\partial T}{\partial t} + \nabla q_C'' = q_p''' - q_{RT}'''} \qquad (4)$$

Where ρ is the quartz density, C_p is the quartz specific heat, e is the thickness of the sample, q_p''' is the volumetric power from the thruster defined as $q_p'''.e.\Sigma_p = q_p''.\Sigma_p$, q_{RT}''' is the volumetric radiative transfer defined as $q_{RT}'''.e.\Sigma_p = q_{RT}''.\Sigma_{RT}$. $\Sigma_{RT} \approx 2\Sigma_p$ is the surface of radiative transfer, and Σ_p the surface where the plasma heat the sample. Here it is implicitly assume that, due to the small sample thickness e, transverse variation of the temperature can be ignored (Characteristic conductive time across sample is ~ 80ms)

For times much smaller than the characteristic longitudinal conductive timescale (Td=20s) the conductive flux is negligible. This allows computing the emissivity (5) with material data and the initial temperature rise of the sample.

$$\boldsymbol{\varepsilon = -\frac{1}{\sigma}\frac{\Sigma_p}{\Sigma_{RT}}e\left(\rho C_p \frac{\partial T}{\partial t} - \frac{q_p''}{e}\right)\frac{1}{T^4 - T_0^4}} \qquad (5)$$

The temperature of the coated sample increases by 0,4K/s around 298 kelvins, as shown in Fig. 7, which give an emissivity $\varepsilon_{Au} = 0.36 \pm 0.17$. With the same process for quartz, we find $\varepsilon_{Quartz} = 0.81 \pm 0.19$. The high uncertainty is due to the temperature measure. In the literature, gold emissivity is in the range 0.02-0.37 and

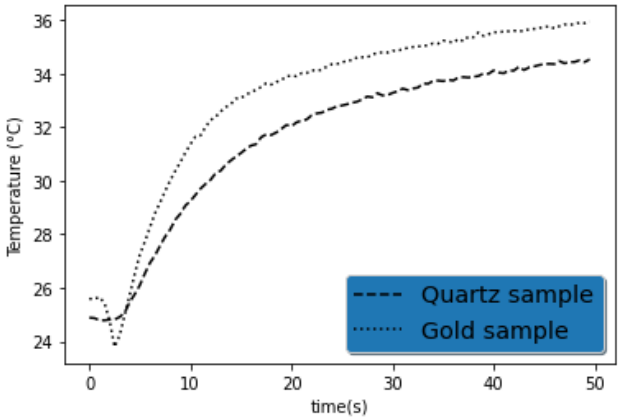

Fig. 7. Temperature change when the quartz or the gold sample are exposed to the ion thruster.

quartz is about 0.75-0.93, [10] [11]. For the gold coating, lowest emissivity is obtained for polished sampled, while the upper value corresponds to unpolished material.

The simulation conditions are listed on TABLE II. As the thermal conductivity of gold is greater than the quartz thermal conductivity, we use an isotemperature hypothesis among the gold layer as the gold diffusivity ($D_{\text{gold}} = 127\text{mm}^2.\text{s}^{-1}$ is one hundred time the quartz diffusivity $D_{\text{quartz}} = 1.4\text{mm}^2.\text{s}^{-1}$).

V. Results

Modal simulations for the reference model give a fundamental frequency $\nu_0 = 33\text{kHz}$, which corresponds to the eigenmode shown in Fig. 6. TABLE IV. gives the change in frequency $\Delta\nu = \nu - \nu_0$ for the different metallized designs. All of these 4 designs have the same fundamental frequency. The expected pressure drift is calculated with the scale factor K_1. It gives also the difference of temperature at different point of the sensor.

The addition of a metallic electrode decreases the temperature gradient across the beam ΔT_{beam} by an order of magnitude, as shown in Fig. 8. A larger metallic electrode decrease it to nearly 0°C. However, the difference of temperature between one end of the vibrating beam and its center $\Delta T_{1/2beam}$ is bigger than ΔT_{beam} for metallic sensor (I - III). The maximal temperature ΔT_{max}, measured by the difference of temperature between hottest point at steady state and the coldest point, increase lightly to 22°C from 15.5°C when gold is added. Then it decreases to 0.4°C for full metallized sensor.

TABLE II. Conditions of Simulation

	Unit	Performances
Heating flux q''_p	mW.cm^{-2}	43
Vacuum casing T_0	°C	25.5
Thermal conductivity	W.m^{-1}.K^{-1}	λ_{quartz}=6-12 Isotemperature for gold
Radiative emissivity		ε_{gold}=0.36 ε_{quartz}=0.81
Mechanical condition		No rotation nor translation of the pads

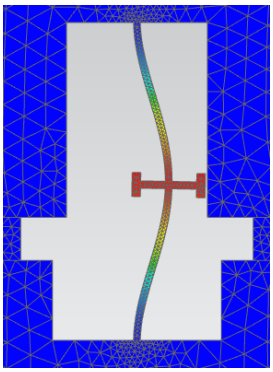

Fig. 6. Fundamental frequency mode of the vibrating beam

The addition of a metallic electrode decreases the temperature gradient across the beam ΔT_{beam} by an order of magnitude, as shown in Fig. 8. A larger metallic electrode decrease it to nearly 0°C. However, the difference of temperature between one end of the vibrating beam and its center $\Delta T_{1/2beam}$ is bigger for metallic sensor than ΔT_{beam}. The maximal temperature ΔT_{max}, measured by the difference of temperature between hottest point at steady state and the coldest point, increase lightly to 22°C from 15,5°C when gold is added. Then it decreases to 0,4°C for full metallized sensor.

The pressure drift can be reduced by the knowledge of the temperature of the vibrating beam and the sensitivity in temperature. The temperature sensitivity of the quartz is determined by applying different temperature to the sensor and monitoring the change in frequency. It gives a flexure sensibility $S_{\text{flexure}} = 0.448\ \text{Hz/°C}$ and a torsional sensibility $S_{\text{torsional}} = 4.95\ \text{Hz/°C}$. As a result, the pressure drift due to the thermal drift decreases on average by 50%. The reference model goes from ~100µN.cm-2 to 40µN.cm-2. The model I keep a high thermal drift at 74 µN.cm-2 while the model III can lower the thermal drift to ~1 µN.cm-2.

TABLE III. Compensation of the Thermal Drift with the Temperature Sensor

	Unit	Ref	I	II	III
Δν	Hz	12.7	17.8	4.8	0.7
Δνtorsional	Hz	58	91	29	6
Δνcorrected	Hz	4.9	9.6	2.2	0.3
ΔPcorrected	µN.cm-2	57.8	74.1	16.9	1.2

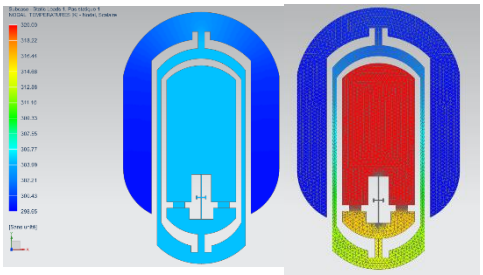

Fig. 8. Temperature gradient of the accelerometer when the plasma hit the proof mass in the case of the original accelerometer RIGHT and metallized accelerometer LEFT.

TABLE IV. RESULTS OF PRESTRESSED MODAL SIMULATION ON THE FOUR MODELS

	Unit	Reference model	I	II	III
$\Delta\nu$	Hz	12.7	17.8	4.8	0.7
Pressure drift ΔP	$\mu N.cm^{-2}$	**98.4**	**138.0**	**37.2**	**5.4**
Difference of temperature between two ends of the vibrating beam ΔT_{beam}	°C	4.4	0.04	0	0
Difference of temperature between one end of the vibrating beam and its center $\Delta T_{1/2\ beam}$	°C	2.2	1.5	0.4	0
Difference of temperature between the hottest and the coldest point ΔT_{max}	°C	15.5	22.0	5.5	0.8

VI. DISCUSSION

The reference model of this quartz sensor shows high thermal drift when exposed to the plasma produced by an ECR thruster. At the distance of 20cm, the estimated pressure produced by the thruster is $6\mu N.cm^{-2}$. With a $60\mu N.cm^{-2}$ thermal drift, it is not possible to measure the thrust.

It is necessary to increase the cooling of the sensor. The use of metallic electrode is a solution because it increases the thermal conductivity. Additionally, this electrode can also evacuate the charges deposited by the plasma. When metal is added to the quartz surface on the model I, the temperature increase. This increase is due to low radiative emissivity of the gold decreasing the radiative cooling while the conductive cooling does not change. For the model II and III, the metal enhances the conductive heat losses thanks to its high thermal conductivity simplified as an iso temperature surface. This increase in conductive transfer is greater than the decrease in radiative transfer. The way to decrease the global temperature of the sensor is to add thermally conductive material like gold all over the surface. The emissivity of the metal has to be the same as the gold emissivity or greater. A lower emissivity will increase the temperature of the sensor and lower its performances mainly in the case of the model I. If the emissivity of gold is changed from 0.36 to 0.19 for the model II, then the temperature of the sensor increases by 30°C instead of 22°C.

The fully metallized sensor III lowers the temperature gradient across the beam to nearly zero. Then the frequency drift is only due to the global temperature of the quartz. With the temperature homogeneity in the sensor, it should be enough to compensate totally the frequency drift. However, it is not the case. A possible reason for this incomplete compensation is inhomogeneous temperature in the quartz temperature sensor. The variation of temperature are less than 0.1°C, which is enough to produce a bias. The thermal pressure drift obtained by this model is $1.2\mu N.cm^{-2}$ corresponding to a thermal drift error of about 20%. This is a great improvement and can allow using this sensor for thrust measurement.

There are three solutions to improve the measure and decrease the thermal measure drift. Firstly, we can decrease the thermal load on the sensor by increasing the distance between the sensor and the ECR thruster or by decreasing the surface of contact between the plasma jet and the proof mass. Secondly, we can increase the radiative transfer by changing the metal layer. Finally, we can increase the conductive cooling. This study shows the disadvantage of the decoupling frame on the thermal cooling. With its long and narrow path, it limits the conductive transfer as in the model I. However, this decoupling frame is necessary to keep a high quality factor for accelerometric measurements for which the sensor was initially designed. By changing completely the design of the sensor, we can remove the decoupling frame and thus cool more efficiently the sensor.

VII. CONCLUSION

A quartz force sensor for electric propulsion thrust measurement have been presented. A study of thermal load shows that the thermal pressure drift in the measurement is ten time the thrust measured at a distance of 20cm. The use of gold electrodes increases the conductive transfer and reduces the thermal drift by an order of magnitude. The use of a quartz temperature sensor mounted directly on the thrust sensor provides an accurate temperature measurement to compensate the thermal drift. The resulting thermal drift error is about 20% of the estimated thrust. Experimental evaluation of the temperature and measured thrust for a coated sensor will be done to confirm these findings. Additionally, different thicknesses and metal coatings will be evaluated to increase sputtering resistance of this electrode.

VIII. AKNOWLEDGMENT

This work has been co-funded by the CNES. The authors would thank Alberto Rossi from CNES for his help.

IX. REFERENCE

[1] J. E. Polk et e. al, «Recommended practice for thrust measurement in electric propulsion testing,» *Journal of Propulsion Power*, vol. 33, n°13, pp. 539-555, 2017.

[2] D. Packan, J. Bonnet et S. Rocca, «Thrust Measurements with the ONERA Micronewton Balance,» 2007. Available: https://www.researchgate.net/publication/242185203. [19 May 2021].

[3] H. Böhrk et M. Auweter-Kurtz, «Thrust Measurement of the Hybrid Electric Thruster TIHTUS by a Baffle Plate,» *Journal of Propulsion Power*, vol. 25, n°13, pp. 729-736, May 2009.

[4] A. Spethmann, T. Trottenberg et H. Kersten, «Spatially Resolved Momentum Flux Measurements for Thruster Plume Diagnostics,» *IEPC*, 2013.

[5] P. Elias, J. Bonnet, J. Jarrige, V. Gaudineau et C. Boniface, «Thrust Measurements using plasma pressure measurements in the plume: a feasibility,» *IEPC*, Vienna, 2019.

[6] T. Vialis, «Development of an electron cyclotron resonance plasma thruster for satellite,» *Thesis*, December 2018.

[7] R. Levy, D. Janiaud, J. Guerard, R. Taibi et O. L. Traon, «A 50 nano-g resolution quartz Vibrating Beam Accelerometer,» *1st IEEE Int. Symp. Inert. Sensors Syst. ISISS 2014*, 2014.

[8] B. Bourgeteau-Verlhac, R. Lévy, P. Lavenus, C. Chartier, V. Gaudineau et O. L. Traon, «High Precision Accelerometer with Integrated Thermal Sensor,» *Proceedings*, 2017.

[9] S. Correyero, J. Jarrige, D. Packan et E. Ahedo, «Plasma beam characterization along the magnetic nozzle of an ECR thruster,» *Plasma Sources Science and Technology*, vol. 28, n°19, 2019.

[10] Transmetra Messtechnik mit KnowHow, «Table of emissivity of various surfaces».

[11] OMEGA, «Table of total emissivity».